ACS central science

Research Article

Cite This: ACS Cent. Sci. 2018, 4, 105−111

$[Ti_8Zr_2O_{12}(COO)_{16}]$ Cluster: An Ideal Inorganic Building Unit for Photoactive Metal−Organic Frameworks

Shuai Yuan,[‡,†] Jun-Sheng Qin,[‡,†] Hai-Qun Xu,[#] Jie Su,[§] Daniel Rossi,[‡] Yuanping Chen,[⊥] Liangliang Zhang,[‡] Christina Lollar,[‡] Qi Wang,[‡] Hai-Long Jiang,*[,#] Dong Hee Son,[‡] Hongyi Xu,[§] Zhehao Huang,*[,§] Xiaodong Zou,[§] and Hong-Cai Zhou*[,‡,∥]

[‡]Department of Chemistry, Texas A&M University, College Station, Texas 77843-3255, United States

[§]Berzelii Centre EXSELENT on Porous Materials and Inorganic and Structural Chemistry, Department of Materials and Environmental Chemistry, Stockholm University, Stockholm 106 91, Sweden

[#]Hefei National Laboratory for Physical Sciences at the Microscale, Collaborative Innovation Center of Suzhou Nano Science and Technology, Department of Chemistry, University of Science and Technology of China, Hefei 230026, P. R. China

[⊥]School of Physics and Optoelectronics, Xiangtan University, Xiangtan 411105, P. R. China

[∥]Department of Materials Science and Engineering, Texas A&M University, College Station, Texas 77843-3003, United States

Supporting Information

ABSTRACT: Metal−organic frameworks (MOFs) based on Ti-oxo clusters (Ti-MOFs) represent a naturally self-assembled superlattice of TiO_2 nanoparticles separated by designable organic linkers as antenna chromophores, epitomizing a promising platform for solar energy conversion. However, despite the vast, diverse, and well-developed Ti-cluster chemistry, only a scarce number of Ti-MOFs have been documented. The synthetic conditions of most Ti-based clusters are incompatible with those required for MOF crystallization, which has severely limited the development of Ti-MOFs. This challenge has been met herein by the discovery of the $[Ti_8Zr_2O_{12}(COO)_{16}]$ cluster as a nearly ideal building unit for photoactive MOFs. A family of isoreticular photoactive MOFs were assembled, and their orbital alignments were fine-tuned by rational functionalization of organic linkers under computational guidance. These MOFs demonstrate high porosity, excellent chemical stability, tunable photoresponse, and good activity toward photocatalytic hydrogen evolution reactions. The discovery of the $[Ti_8Zr_2O_{12}(COO)_{16}]$ cluster and the facile construction of photoactive MOFs from this cluster shall pave the way for the development of future Ti-MOF-based photocatalysts.

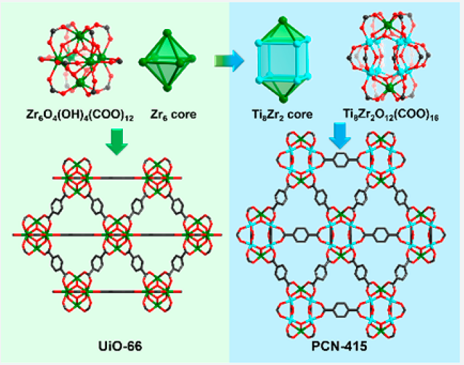

INTRODUCTION

Mimicking natural photosynthesis using artificial chemical systems to harness solar energy is an appealing alternative to address increasing global energy demands and dwindling fossil fuel supplies.[1] Since the discovery of water splitting on TiO_2 photoelectrodes by Fujishima and Honda in 1972,[2] researchers have been attempting to develop artificial systems to perform similar photochemical reactions using simple inorganic and/or organic materials.[3,4] Although a large number of materials have already been explored, TiO_2 is still considered one of the most successful photocatalysts due to its high efficiency, chemical stability, earth abundance, and relatively low toxicity.[5]

Among the numerous photocatalytic systems, metal−organic frameworks (MOFs) are a unique class of materials owing to their crystalline nature, high porosity, and tunable functionality.[6−9] Highly crystalline MOF structures represent a naturally self-assembled superlattice of metal oxide nanoparticles in which identical metal oxide clusters are stabilized from coalescence by connecting ligands. The distance and orientation of metal oxide clusters can be precisely determined via X-ray crystallography, allowing for theoretical prediction of electronic coupling and energy transfer. The optical response, electronic valence, and conduction level alignment of MOFs can be fine-tuned by judicious selection of specific metal oxide nodes and photoactive organic linkers. Most importantly, the designable cluster-linker arrangement potentially mimics the photosystems, in which photon collection and subsequent energy transfer are realized by highly ordered pigment−protein complexes. Similarly, the structural motifs for photosensitization and catalytic sites can be constructed in close proximity within MOFs where short-lived electrons and holes can be consumed before recombination. Additionally, the porosity of MOFs facilitates the diffusion of substrates and products through MOF channels, making them ideal heterogeneous photocatalysts.[10] Therefore, the application of MOFs in heterogeneous photocatalysis for hydrogen generation, CO_2

Received: October 17, 2017
Published: November 29, 2017

DOI: 10.1021/acscentsci.7b00497
ACS Cent. Sci. 2018, 4, 105−111

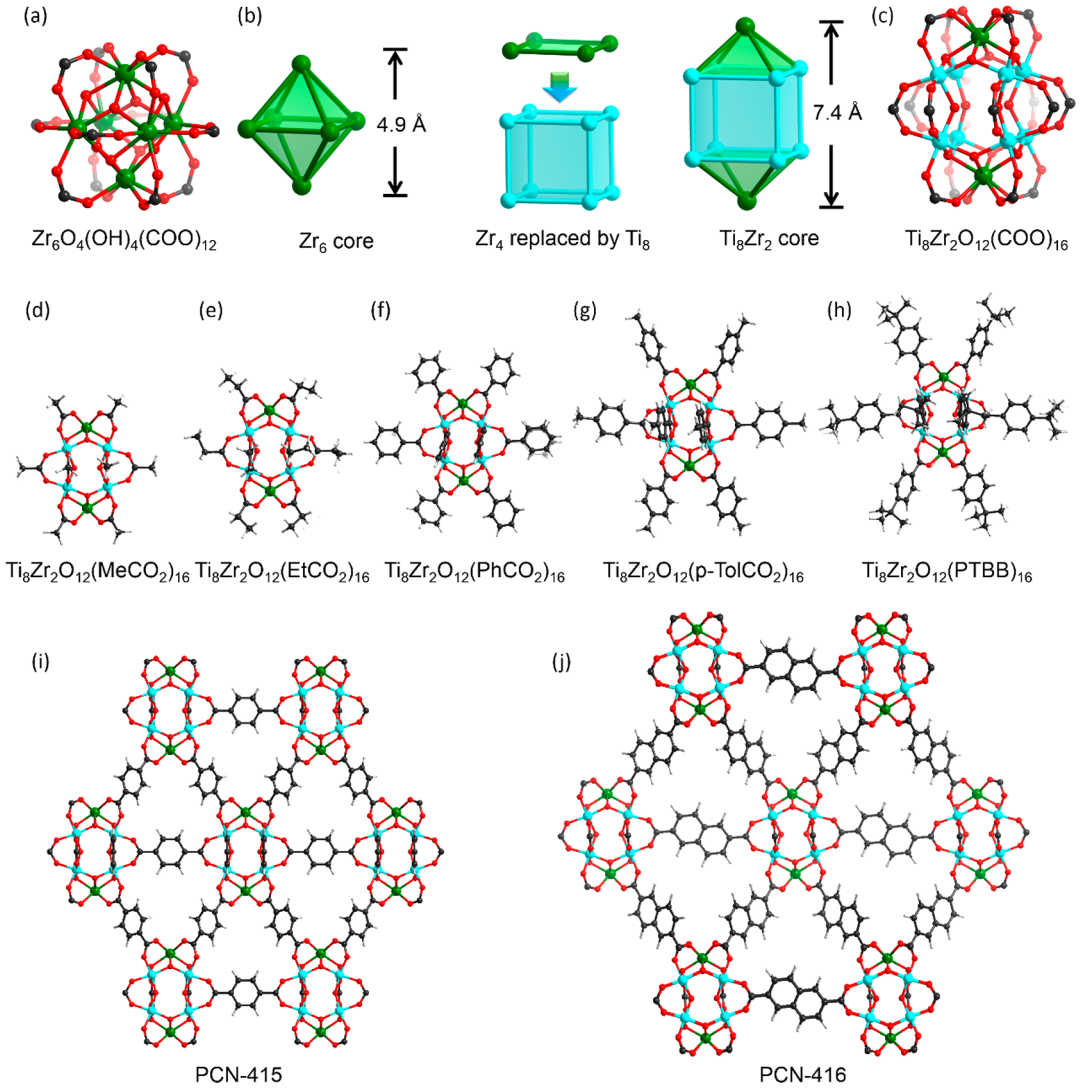

Figure 1. Coordination compounds based on $[Ti_8Zr_2O_{12}(RCOO)_{16}]$ cluster. (a) $[Zr_6O_4(OH)_4(COO)_{12}]$ cluster; (b) the relationship between $[Zr_6O_4(OH)_4(COO)_{12}]$ and $[Ti_8Zr_2O_{12}(COO)_{16}]$ clusters; (c) $[Ti_8Zr_2O_{12}(COO)_{16}]$ cluster; (d–h) discrete $[Ti_8Zr_2O_{12}(RCOO)_{16}]$ clusters formed with different carboxylate ligands; (i) and (j) MOFs based on $[Ti_8Zr_2O_{12}(RCOO)_{16}]$ clusters and different carboxylate linkers.

reduction, and organic transformations has attracted increasing attention in recent years.[11]

In this context, Ti-oxo clusters, with good chemical stability, redox activity, and photocatalytic properties, appear to be attractive building units to construct photoactive MOFs.[12] The tetravalent Ti^{4+} cation tends to form strong coordination bonds with carboxylate linkers, ensuring framework stability and structural intactness during catalytic reactions. The titanium-oxo clusters act as analogues of TiO_2 nanoparticles, which endow the titanium-oxo-based MOF with photocatalytic activity.[13,14] Although they are highly desired, only a few examples of Ti-MOFs have been reported to date.[13,15−20] One representative example is MIL-125,[13] which has been extensively studied as a photocatalyst for water reduction,[21] CO_2 reduction,[22] and organic transformations.[23] The synthetic challenges of Ti-MOFs are attributed to the sensitivity of Ti-clusters to reaction conditions, and in many cases, the incompatibility of cluster formation conditions with those required for MOF crystallization. On the other hand, the robust hexa-nuclear $[Zr_6O_4(OH)_4(COO)_{12}]$ cluster has allowed for the design and construction of various Zr-MOFs through isoreticular chemistry.[24,25] However, the catalytic performance of Zr-MOFs is far below that of their Ti-based analogues due to the short excitation state lifetime and severe charge recombination.[26] This encourages us to discover a suitable cluster to construct a photoactive MOF system that combines the advantages of Zr-MOFs (i.e., facile design and synthesis) and Ti-MOFs (i.e., high photoactivity). While existing Ti-oxo clusters or Zr-oxo clusters in the literature do not meet these requirements, a combination of two metals into a bimetallic cluster has brought new opportunities. For the first time, we synthesized the $[Ti_8Zr_2O_{12}(COO)_{16}]$ cluster as a Ti-containing analogue of the $[Zr_6O_4(OH)_4(COO)_{12}]$ cluster. Furthermore, the $[Ti_8Zr_2O_{12}(COO)_{16}]$ cluster can be easily extended into a series of photoactive MOFs under the guidance of reticular chemistry.

RESULTS AND DISCUSSION

$[Ti_8Zr_2O_{12}(RCOO)_{16}]$ Clusters. As reflected by the large number of Ti-oxo-clusters in the literature, the cluster chemistry of Ti^{4+} is rich and versatile.[27] Indeed, carboxylate-based Ti-oxo-clusters show a large panel of nuclearities and

DOI: 10.1021/acscentsci.7b00497
ACS Cent. Sci. 2018, 4, 105−111

geometries, depending on the synthetic conditions such as the metal/ligand ratio, solvent, reaction time, temperature, and pressure. Although numerous molecular Ti-clusters have been documented, it has been difficult to directly utilize them as starting building blocks for MOF synthesis.[12] The main reason is the sensitivity of cluster formation to reaction conditions, and, in many cases, the incompatibility of such conditions with those required for MOF synthesis and crystallization.[14] For example, many Ti-oxo-clusters crystallize in acetonitrile or methanol, whereas *N*,*N*-dimethylformamide (DMF) is usually required as solvent for the synthesis of MOFs. In addition, some Ti-oxo-clusters terminated by alkoxides are water-sensitive which are prone to undergo fast and spontaneous hydrolysis during MOF synthesis. These limitations have largely prevented the incorporation of vast, diverse Ti-oxo-clusters into MOF structures.

In contrast, the $[Zr_6O_4(OH)_4(COO)_{12}]$ cluster (Figure 1a) has been shown to be a nearly ideal inorganic building unit for the construction of MOFs.[24] Various MOFs based on the $[Zr_6O_4(OH)_4(COO)_{12}]$ cluster have been synthesized under similar synthetic conditions.[25,28−31] This encourages us to find a Ti-containing cluster with behavior similar to $[Zr_6O_4(OH)_4(COO)_{12}]$ for MOF synthesis.[32] Efforts were made in our group to build Ti-MOFs using existing Ti-oxo clusters in the literature but to no avail. These clusters tend to dissociate or transform during the MOF synthesis.[15] While existing monometallic clusters do not meet the requirement for MOF synthesis, bimetallic clusters have brought new opportunities. During our continued interest in cluster chemistry, a $[Ti_8Zr_2O_{12}(COO)_{16}]$ cluster (Figure 1c) was discovered as a promising inorganic building unit for MOF synthesis.

The $[Ti_8Zr_2O_{12}(RCOO)_{16}]$ (R = Me, Et, Ph, p-Tol and PTBB) clusters (Figure 1d−h) were synthesized by the solvothermal reactions of Zr^{4+}, Ti^{4+}, and an excess amount of carboxylic acids (Figure S1), similar to the synthetic conditions for $[Zr_6O_4(OH)_4(RCOO)_{12}]$ clusters and most Zr-MOFs. Single crystals were successfully isolated for all the $[Ti_8Zr_2O_{12}(RCOO)_{16}]$ (R = Me, Et, Ph, p-Tol, and PTBB) clusters (Table S1). Structure analysis reveals that the bimetallic decanuclear cluster is composed of a Ti_8-cube capped by two Zr^{4+} centers on the top and bottom. Four μ_2-O rest on the equatorial plane, each bridging a pair of Ti^{4+} to form a $[Ti_8O_4]^{24+}$ center. Two Zr^{4+} on the top and bottom were further connected to the $[Ti_8O_4]^{24+}$ center by eight μ_3-O, generating the $[Ti_8Zr_2O_{12}]^{16+}$ core. The $[Ti_8Zr_2O_{12}]^{16+}$ core was terminated by 16 carboxylates fulfilling a neutral $[Ti_8Zr_2O_{12}(COO)_{16}]$ cluster (Figure 1c). In fact, the $[Ti_8Zr_2O_{12}(COO)_{16}]$ cluster is structurally related to the $[Zr_6O_4(OH)_4(COO)_{12}]$ cluster (Figure 1b). It can be derived from the $[Zr_6O_4(OH)_4(COO)_{12}]$ cluster by replacing four equatorial Zr^{4+} by a Ti_8-cube. As a result, four carboxylate ligands within the equatorial plane that bridges the Zr_4-square are replaced by eight carboxylate ligands perpendicular to the equatorial plane, which bridges the Ti_8-cube.

Interestingly, the $[Ti_8Zr_2O_{12}(RCOO)_{16}]$ (R = Me, Et, Ph, p-Tol, and PTBB) clusters are dominating products under a variety of conditions. They tolerate the modification of substituents with different sizes on the carboxylate linker and the variation of synthetic conditions without altering the $[Ti_8Zr_2O_{12}]^{16+}$ core structure. For example, the $[Ti_8Zr_2O_{12}(PhCOO)_{16}]$ cluster can be obtained regardless of the solvents (DMF, methanol, and acetonitrile), temperatures (from 80 to 150 °C), and Ti/Zr ratios (from 1 to 10), as long as the carboxylic acid is in excess. Therefore, the robust $[Ti_8Zr_2O_{12}(COO)_{16}]$ cluster represents a nearly ideal Ti-containing substitute of the $[Zr_6O_4(OH)_4(COO)_{12}]$ cluster for the construction of photoactive MOFs.

$[Ti_8Zr_2O_{12}(COO)_{16}]$ Cluster-based MOFs. The solvothermal reaction between the $[Ti_8Zr_2O_{12}(MeCOO)_{16}]$ cluster and BDC (1,4-benzenedicarboxylate) gives rise to the desired MOF, PCN-415 (Figures 1i and S2), under similar synthetic conditions used for the syntheses of Zr-MOFs. The acetate terminated $[Ti_8Zr_2O_{12}(MeCOO)_{16}]$ cluster was adopted as the starting material because of its good solubility in DMF. The preformed cluster as starting material is the key for the formation of pure PCN-415 because it eliminates numerous competing side reactions. For comparison, the synthesis of PCN-415 was attempted using a mixture of stoichiometric Zr^{4+} and Ti^{4+} metal salts which leads to low crystallinity PCN-415 with UiO-66 impurity. In addition, an excess amount of carboxylic acid as modulating reagent is also necessary for the formation of a highly crystalline product. The carboxylic acid acts as a modulator that competitively coordinates with the metals and slows down crystal growth to help produce highly crystalline products. Furthermore, isoreticular expansion of PCN-415 can be realized by elongation of BDC into 2,6-naphthalenedicarboxylate (NDC), which gives rise to an isoreticular MOF, PCN-416 (Figures 1j and S3).

Since the crystal sizes of PCN-415 and −416 are too small for single crystal X-ray diffraction, their structures are directly solved from continuous rotation electron diffraction (*c*RED) and confirmed by Rietveld refinement against synchrotron PXRD data (Figure 2, see Supporting Information for Rietveld refinement details). The structure models refined against *c*RED and PXRD show excellent agreement with each other, and the atomic positions differ on average only by 0.032 Å for Zr/Ti and by 0.071 Å for O/C (Tables S2−S5). In the crystal structure of PCN-415, each $[Ti_8Zr_2O_{12}(COO)_{16}]$ cluster (Figure 3a) is connected to 16 linear BDC linkers (Figure

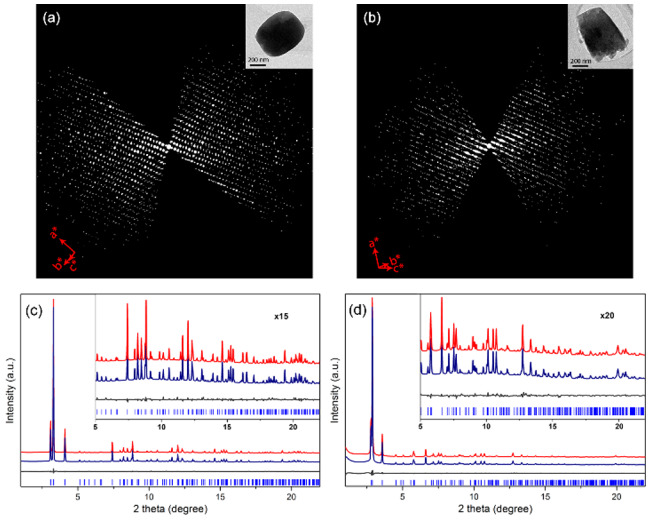

Figure 2. Reconstructed 3D reciprocal lattice and Rietveld refinement. Reconstructed 3D reciprocal lattice of (a) PCN-415 and (b) PCN-416 from *c*RED data. Inset is the crystal from which the RED data were collected. PXRD Rietveld refinement of (c) PCN-415 and (d) PCN-416 displaying the observed pattern (navy), calculated pattern (red), difference plot (gray), and Bragg positions (blue bars) (λ = 0.72768 Å).

DOI: 10.1021/acscentsci.7b00497
ACS Cent. Sci. 2018, 4, 105−111

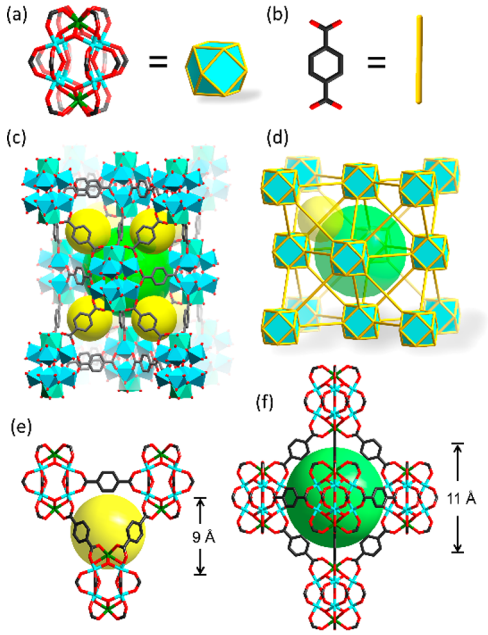

Figure 3. Structural analysis. Topological simplification of (a) the $[Ti_8Zr_2O_{12}(COO)_{16}]$ cluster and (b) the BDC linker; (c) crystal structure and (d) topological presentation of PCN-415 as an **fcu** net; (e) small tetrahedral cage and (f) large octahedral cage in PCN-415.

3b) to form a three-dimensional (3D) framework (Figure 3c). There is a tetragonal cage with a diameter of 9 Å and an octahedral cage with a diameter of 11 Å (Figure 3e,f). Two types of symmetrically independent BDC linkers are observed. Topologically, a pair of parallel BDC linkers within the equatorial plane is regarded as one edge. Therefore, eight equatorial BDC linkers are simplified into four edges. On the other hand, eight BDC linkers above and below the equatorial plane are simplified into eight edges. As a result, the $[Ti_8Zr_2O_{12}(COO)_{16}]$ cluster acts as a 12-connected node, affording a network with **fcu** topology (Figure 3d).[33−36] PCN-416 is isoreticular to PCN-415 with the same $[Ti_8Zr_2O_{12}(COO)_{16}]$ cluster and elongated linkers. The distance between each pair of parallel NDC linkers is 3.5 Å, indicating a $\pi-\pi$ interaction between naphthalene moieties. A small tetragonal cage and large octahedral cage were observed in PCN-416 with diameters of 11 and 13 Å, respectively. Since PCN-416 is an isoreticular expansion of PCN-415, they share the same **fcu** topology.

Porosity and Stability. The porosity of PCN-415 and PCN-416 is estimated by N_2 sorption measurements at 77 K. Both PCN-415 and PCN-416 are highly porous with BET surface areas of 1050 and 1337 $m^2 \cdot g^{-1}$ (Figures S6 and S7), respectively. More importantly, PCN-415 and PCN-416 exhibit excellent chemical stabilities in aqueous solutions with a wide pH range for at least 24 h. The N_2 adsorption isotherms (Figures S8 and S9) and PXRD patterns (Figures S10 and S11) of MOF samples are not altered after stability tests, indicating maintained crystallinity and intact porosity. The remarkable chemical stability of PCN-415 and PCN-416 can be attributed to the strong $M^{4+}-O$ (M = Ti or Zr) bond and the highly connected cluster, which resist the attack of water and other guest species.

Engineering of Optical Response. The optical band gap of PCN-415 was calculated to be 3.3 eV based on the UV−vis spectrum (Figure S15a), indicating no adsorption in the visible light range. This has limited the application of PCN-415 in visible-light-induced catalysis. The amine-functionalized BDC linkers were reported to provide an extra absorption band in the visible region, which has been encountered in UiO-66[37,38] and MIL-125.[22,39] Therefore, the optical response of PCN-415 was tuned by introducing amino groups on the BDC linker.

PCN-415 with different concentrations of monoaminated BDC-NH_2 (2-aminoterephthalate, Figure S12) was synthesized by varying the ratios of BDC-NH_2 in the starting material (i.e., 30%, 50%, 70%, and 100%). The resulting MOFs were named PCN-415-$(NH_2)_{0.3}$, PCN-415-$(NH_2)_{0.5}$, PCN-415-$(NH_2)_{0.7}$, and PCN-415-NH_2, respectively. In addition, the diamine functionalized PCN-415-$(2NH_2)_{0.5}$ was also synthesized by introducing 50% of diaminated BDC-$2NH_2$ (2,5-diaminoterephthalate). The amine functionalized derivatives possess the same structure as PCN-415 as suggested by PXRD patterns (Figure S13) and N_2 adsorption isotherms (Figures 4a and

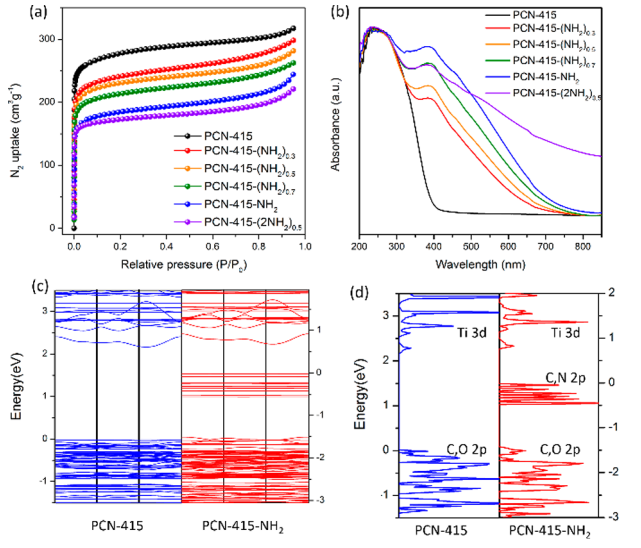

Figure 4. Engineering the optical response of PCN-415. (a) N_2 adsorption isotherms, (b) UV−vis spectra, (c) DFT calculated band structures, and (d) DOSs for PCN-415 and PCN-415-NH_2.

S14). UV−vis spectra indicate an obvious red shift of absorption peaks and a reduction of band gap upon the introduction of amino groups (Figure 4b). The absorption onsets (from 544 to 623 nm) and band gaps (from 2.28 to 1.99 eV) do not largely vary for all of the monoaminated samples, but the molar extinction coefficient notably increased with increasing BDC-NH_2 contents (Figure S15b). This feature was reflected in the physical appearance, which shows increased yellow color intensity with increasing amount of BDC-NH_2. The diamine functionalized sample, PCN-415-$(2NH_2)_{0.5}$, shows a further band gap decrease with an optical band gap of 1.2 eV (Figure S15c), shifting the absorption onset to the red/IR region. The flat-band potential of PCN-415 and its amine functionalized derivatives are similar (~0.5 eV) as determined by the Mott−Schottky plots (Figure S16). PCN-416, with naphthalene moieties, have inherent visible light absorption (Figures S17 and S18). The band gap of PCN-416 could be further narrowed by introducing amino groups on the NDC linker (Figures S19 and S20). The photocurrent response of PCN-415 toward visible light also increased by the amino groups (Figure S21).

DOI: 10.1021/acscentsci.7b00497
ACS Cent. Sci. 2018, 4, 105−111

To understand the origin of band gap reduction by amino functionalization, electronic structure calculations were performed for PCN-415 and its derivatives using density functional theory (DFT). The calculated band gap of PCN-415 is larger than that of PCN-415-NH_2 indicating that the introduction of -NH_2 decreases the band gap. By shifting the Fermi level to align the conduction band minimums (CBMs) of the two structures, one can find that the band gap decrease is attributed to the midgap flat bands generated in PCN-415-NH_2 (Figure 4c). The comparison of density of states (DOSs) for PCN-415 and PCN-415-NH_2 further illustrates this point (Figure 4d). The upper valence bands (VBs) are composed of BDC aromatic 2p orbitals, while bottom conduction bands (CBs) are dominated by the Ti 3d orbitals. Therefore, the excitation of PCN-415 by UV light transfers the electron from VBs at BDC to CBs at Ti, corresponding to the ligand to metal charge transfer (LMCT). Introducing amino groups on the BDC linker pushes the VB into a high energy occupied state. Midgap states were introduced into the band gap that corresponded to the N and C 2p orbitals from BDC-NH_2 (Figure S22a–c). On the other hand, the CBs are minimally affected by the amino groups on the linkers, which matched well with the Mott–Schottky plots. This phenomenon is a close remittance of the N doped TiO_2 in which the N 2p orbital created the midgap band to narrow the overall band gap. The diamine functionalized sample shows further reduced band gap because of the strong electron donating characteristics of aromatic diamines (Figure S22d). The contributions of ligand orbitals to the CBs are also increased in the diamine functionalized sample, suggesting an increased proportion of ligand based excitation as compared to LMCT. The calculated band gap of PCN-416 is inherently smaller than that of PCN-415, which was further reduced by amino functionalization (Figure S22). Overall, the localized electronic modification results in flat bands in k-space, indicating the absence of long-range interactions. The CBM and valence band maximum (VBM) in MOFs can be regarded as the lowest unoccupied and highest occupied molecular orbitals (LUMO and HOMO), respectively. Although the terms for semiconductors (VB, CB, and band gap) have been commonly used to describe MOFs, theoretical studies indicated the insulating nature of PCN-415, as suggested by the localized electronic states.

Photochemical Hydrogen Production. With the high porosity, excellent chemical stability, tunable optical response, and photoactive clusters, PCN-415 and PCN-416 provide ideal platforms for the design of MOF photocatalysts. As a proof of concept, the photochemical hydrogen production catalyzed by PCN-415 and its derivatives was tested. The photocatalytic hydrogen generation was performed in acetonitrile and H_2O with triethanolamine (TEOA) as a sacrificial agent and Pt nanoparticles as cocatalysts under 300 W Xe lamp equipped with a UV cutoff filter (λ > 380 nm) (Figure S23). The formation of H_2 was detected by gas chromatography (GC). No H_2 was detected in the dark showing the photocatalytic nature of the reaction. The inactivity of the parent PCN-415 under the same conditions confirms that the photocatalytic activity is attributed to the amino functionality. The H_2 generation efficiency notably increased with the BDC-NH_2 content and then leveled off. Among all the tested materials, PCN-415-NH_2 shows the highest activity with an H_2 evolution rate of 594 μmol g^{-1} h^{-1} (Table 1). To test the photocatalytic stability of PCN-415-NH_2, cycling experiments were conducted. The catalytic activity was well-maintained after three cycles (Table S6). The PXRD patterns after the photocatalytic reaction reveal the stability of PCN-415 during the reaction (Figure S24). Although the diamine functionalized samples have small band gaps and strong visible light absorption, they show relatively low activity. In fact, the excitations of PCN-415-$(2NH_2)_{0.5}$ and PCN-416-$(2NH_2)_{0.5}$ are more ligand-based instead of LMCT, which have a short lifetime accounting for the low catalytic performance. This is in line with the computational results, which suggested significant contributions of ligand orbitals to both VBs and CBs. Therefore, the photocatalytic activity of MOFs cannot be directly correlated with band gaps. For comparison, the performance of UiO-66-NH_2 was also tested as a Zr-only analogue of PCN-415-NH_2 which showed much lower activity (Table S7). This result highlights the effect of Ti^{4+} in PCN-415 as a photoactive species for photochemical hydrogen production.

Table 1. Catalytic Performance of MOFs in the Photocatalytic Hydrogen Generation[a]

entry	photocatalysis	H_2 (μmol·g^{-1}·h^{-1})
1	PCN-415	44
2	PCN-415-$(NH_2)_{0.3}$	469
3	PCN-415-$(NH_2)_{0.5}$	503
4	PCN-415-$(NH_2)_{0.7}$	514
5	PCN-415-NH_2	594
6	PCN-415-$(2NH_2)_{0.5}$	130
7	PCN-416	484
8	PCN-416-$(2NH_2)_{0.5}$	51
9	UiO-66-NH_2	94

[a]Reaction conditions: 5 mg of catalyst, 28 mL of CH_3CN, 2 mL of TEOA, 200 μL of H_2O, 50 μg of Pt, 300 W Xe lamp with a UV cutoff filter (λ > 380 nm), 4 h.

In order to investigate the nature of excited states in the PCN-415-NH_2, we carried out transient absorption spectroscopy (TAS) and electron paramagnetic resonance (EPR) spectroscopy measurements. For EPR studies, PCN-415-NH_2 was subjected to conditions similar to those during photocatalytic reaction but without Pt cocatalysts. Illuminating PCN-415-NH_2 leads to the appearance of an intense paramagnetic signal ascribed to Ti^{3+} (Figure S25). This is in line with the observation that the color of the reaction suspension changes from the original yellow to green upon light irradiation, and quickly changed back upon exposure to O_2 (Figure S26). UiO-66-NH_2 exposed to the same conditions did not develop any additional paramagnetic features upon illumination. The EPR results suggest that light irradiation promotes transfer of photogenerated electrons from the excited BDC-NH_2 to the $[Ti_8Zr_2O_{12}(COO)_{16}]$ cluster, resulting in the formation of Ti^{3+} species. Transient absorption spectroscopy (TAS) was further applied to study the lifetime of the excited states. Excitation of PCN-415-NH_2 at 400 nm results in an intense transient signal with a maximum at 580 nm with a moderately long lifetime of up to 9 ns (Figure S27). For comparison, the UiO-66-NH_2 shows a broad transient signal at 750 nm which decays rapidly within 10 ps. The main difference between the PCN-415-NH_2 and UiO-66-NH_2 is the occurrence of absorption bands at much lower wavelengths, which is tentatively assigned to the stabilized holes on the linker and the formation of Ti^{3+} species.

On the basis of these results and literature, an LMCT mechanism was proposed for the hydrogen generation reaction (Figure S28). The BDC-NH_2 linkers serve as antennas to absorb light and transfer the photoexcited electrons to the

DOI: 10.1021/acscentsci.7b00497
ACS Cent. Sci. 2018, 4, 105–111

$[Ti_8Zr_2O_{12}(COO)_{16}]$ cluster forming Ti^{3+} species. The photogenerated electrons on the Ti^{3+} were then transferred to the Pt surface where the proton reduction takes place. Meanwhile, the photogenerated holes on the BDC-NH_2 linkers were reduced by TEOA as electron donors, fulfilling the catalytic cycle. The remarkable difference between PCN-415-NH_2 and UiO-66-NH_2 in photocatalytic activity is therefore explained by the stabilized excited state of PCN-415-NH_2 by the formation of Ti^{3+}, whereas the UiO-66-NH_2 does not promote the formation of corresponding intermediates. Previously reported computational results also indicate that the HOMO−LUMO transitions of UiO-66-NH_2 are purely ligand-based as the d-orbitals of Zr do not overlap with the π^* orbital of the ligand. In contrast, LMCT can be achieved in PCN-415-NH_2 to allow long-lived charge separation and efficient utilization of the photogenerated electrons. These results signify the importance of Ti^{4+} on the excitation lifetime and photocatalytic performance in hydrogen production reactions.

CONCLUSIONS

In conclusion, we have discovered a $[Ti_8Zr_2O_{12}(COO)_{16}]$ cluster as an inorganic building unit for the preparation of a series of isoreticular photoactive MOFs. The resulting MOFs, namely, the PCN-415 and PCN-416 series, demonstrate high porosity, excellent chemical stability, tunable photoresponsivity, and good catalytic activity toward water reduction. We expect that the $[Ti_8Zr_2O_{12}(COO)_{16}]$ cluster will act as a Ti-containing replacement of the $[Zr_6O_4(OH)_4(COO)_{12}]$ cluster, which promises the construction of various robust and photoactive MOFs. In addition, the facile synthesis of versatile Ti-containing MOFs shall accelerate the development of MOF-based photocatalysts.

ASSOCIATED CONTENT

Supporting Information

The Supporting Information is available free of charge on the ACS Publications website at DOI: 10.1021/acscentsci.7b00497.

Experimental details, PXRD, gas sorption, ^1H NMR, SEM/TEM, ICP-MS, EPR, transient absorption studies, structure refinement, photocatalytic H_2 production, and DFT calculations (PDF)

CIF files for $[Ti_8Zr_2O_{12}(RCOO)_{16}]$ (R = Me, Et, Ph, p-Tol, and PTBB) clusters (CIF)

AUTHOR INFORMATION

Corresponding Authors

*(H.-L.J.) E-mail: jianglab@ustc.edu.cn.
*(Z.H.) E-mail: zhehao.huang@mmk.su.se.
*(H.-C.Z.) E-mail: zhou@chem.tamu.edu.

ORCID

Yuanping Chen: 0000-0001-5349-3484
Hai-Long Jiang: 0000-0002-2975-7977
Dong Hee Son: 0000-0001-9002-5188
Hong-Cai Zhou: 0000-0002-9029-3788

Author Contributions

†S.Y. and J.-S.Q. contributed equally to this work.

Notes

The authors declare no competing financial interest.

ACKNOWLEDGMENTS

The gas adsorption−desorption studies of this research was supported by the Center for Gas Separations Relevant to Clean Energy Technologies, an Energy Frontier Research Center funded by the U.S. Department of Energy, Office of Science, Office of Basic Energy Sciences under Award Number DE-SC0001015. Structural analyses were supported by the 3DEM-NATUR project from the Knut and Alice Wallenberg Foundation (KAW) and the MATsynCELL project through Röntgen-Ångström Cluster, the Swedish Research Council (VR). Photocatalytic studies were supported by Natural Science Foundation of China (Nos. 21673213, 21371162, and 21521001) and the 973 program (No. 2014CB931803). This computational work was funded by National Natural Science Foundation of China (Nos. 51376005 and 11474243). The authors also acknowledge the financial support of U.S. Department of Energy, Office of Fossil Energy, National Energy Technology Laboratory (DE-FE0026472), Robert A. Welch Foundation (A-0030), and National Science Foundation Small Business Innovation Research (NSF-SBIR) under Grant No. 1632486. Use of the Advanced Photon Source, an Office of Science User Facility operated for the U.S. Department of Energy, Office of Science by Argonne National Laboratory, was supported by the U.S. Department of Energy under Award Number DE-AC02-06CH11357. The Distinguished Scientist Fellowship Program (DSFP) at KSU is gratefully acknowledged for supporting this work. S.Y. acknowledges the Dow Chemical Graduate Fellowship. This material is also based upon work supported by the National Science Foundation Graduate Research Fellowship under Grant No. DGE: 1252521.

REFERENCES

(1) Lewis, N. S.; Nocera, D. G. Powering the planet: Chemical challenges in solar energy utilization. *Proc. Natl. Acad. Sci. U. S. A.* **2006**, *103* (43), 15729−15735.

(2) Fujishima, A.; Honda, K. Electrochemical photolysis of water at a semiconductor electrode. *Nature* **1972**, *238* (5358), 37−38.

(3) Walter, M. G.; Warren, E. L.; McKone, J. R.; Boettcher, S. W.; Mi, Q.; Santori, E. A.; Lewis, N. S. Solar water splitting cells. *Chem. Rev.* **2010**, *110* (11), 6446−6473.

(4) Paracchino, A.; Laporte, V.; Sivula, K.; Grätzel, M.; Thimsen, E. Highly active oxide photocathode for photoelectrochemical water reduction. *Nat. Mater.* **2011**, *10* (6), 456−461.

(5) Chen, X.; Shen, S.; Guo, L.; Mao, S. S. Semiconductor-based photocatalytic hydrogen generation. *Chem. Rev.* **2010**, *110* (11), 6503−6570.

(6) Li, H.; Eddaoudi, M.; O'Keeffe, M.; Yaghi, O. M. Design and synthesis of an exceptionally stable and highly porous metal-organic framework. *Nature* **1999**, *402* (6759), 276−279.

(7) Guillerm, V.; Kim, D.; Eubank, J. F.; Luebke, R.; Liu, X.; Adil, K.; Lah, M. S.; Eddaoudi, M. A supermolecular building approach for the design and construction of metal-organic frameworks. *Chem. Soc. Rev.* **2014**, *43* (16), 6141−6172.

(8) O'Keeffe, M.; Yaghi, O. M. Deconstructing the crystal structures of metal-organic frameworks and related materials into their underlying nets. *Chem. Rev.* **2012**, *112* (2), 675−702.

(9) Kitagawa, S. Future porous materials. *Acc. Chem. Res.* **2017**, *50* (3), 514−516.

(10) Chughtai, A. H.; Ahmad, N.; Younus, H. A.; Laypkov, A.; Verpoort, F. Metal-organic frameworks: versatile heterogeneous catalysts for efficient catalytic organic transformations. *Chem. Soc. Rev.* **2015**, *44* (19), 6804−6849.

(11) Zhang, T.; Lin, W. Metal-organic frameworks for artificial photosynthesis and photocatalysis. *Chem. Soc. Rev.* **2014**, *43* (16), 5982−5993.

DOI: 10.1021/acscentsci.7b00497
ACS Cent. Sci. 2018, 4, 105−111

(12) Assi, H.; Mouchaham, G.; Steunou, N.; Devic, T.; Serre, C. Titanium coordination compounds: from discrete metal complexes to metal-organic frameworks. *Chem. Soc. Rev.* **2017**, *46* (11), 3431−3452.
(13) Dan-Hardi, M.; Serre, C.; Frot, T.; Rozes, L.; Maurin, G.; Sanchez, C.; Ferey, G. A new photoactive crystalline highly porous titanium(IV) dicarboxylate. *J. Am. Chem. Soc.* **2009**, *131* (31), 10857−10859.
(14) Nguyen, H. L.; Gandara, F.; Furukawa, H.; Doan, T. L. H.; Cordova, K. E.; Yaghi, O. M. A titanium-organic framework as an exemplar of combining the chemistry of metal- and covalent-organic frameworks. *J. Am. Chem. Soc.* **2016**, *138* (13), 4330−4333.
(15) Yuan, S.; Liu, T. F.; Feng, D. W.; Tian, J.; Wang, K. C.; Qin, J. S.; Zhang, Q.; Chen, Y. P.; Bosch, M.; Zou, L. F.; Teat, S. J.; Dalgarno, S. J.; Zhou, H. C. A single crystalline porphyrinic titanium metal-organic framework. *Chem. Sci.* **2015**, *6* (7), 3926−3930.
(16) Bueken, B.; Vermoortele, F.; Vanpoucke, D. E. P.; Reinsch, H.; Tsou, C.-C.; Valvekens, P.; De Baerdemaeker, T.; Ameloot, R.; Kirschhock, C. E. A.; Van Speybroeck, V.; Mayer, J. M.; De Vos, D. A flexible photoactive titanium metal−organic framework based on a $[Ti(IV)_3(\mu_3\text{-}O)(O)_2(COO)_6]$ Cluster. *Angew. Chem.* **2015**, *127* (47), 14118−14123.
(17) Nguyen, H. L.; Vu, T. T.; Le, D.; Doan, T. L. H.; Nguyen, V. Q.; Phan, N. T. S. A titanium−organic framework: engineering of the band-gap energy for photocatalytic property enhancement. *ACS Catal.* **2017**, *7* (1), 338−342.
(18) Gao, J.; Miao, J.; Li, P.-Z.; Teng, W. Y.; Yang, L.; Zhao, Y.; Liu, B.; Zhang, Q. A p-type Ti(IV)-based metal-organic framework with visible-light photo-response. *Chem. Commun.* **2014**, *50* (29), 3786−3788.
(19) Assi, H.; Pardo Pérez, L. C.; Mouchaham, G.; Ragon, F.; Nasalevich, M.; Guillou, N.; Martineau, C.; Chevreau, H.; Kapteijn, F.; Gascon, J.; Fertey, P.; Elkaim, E.; Serre, C.; Devic, T. Investigating the case of titanium(IV) carboxyphenolate photoactive coordination polymers. *Inorg. Chem.* **2016**, *55* (15), 7192−7199.
(20) Mason, J. A.; Darago, L. E.; Lukens, W. W.; Long, J. R. Synthesis and O_2 reactivity of a titanium(III) metal−organic framework. *Inorg. Chem.* **2015**, *54* (20), 10096−10104.
(21) Horiuchi, Y.; Toyao, T.; Saito, M.; Mochizuki, K.; Iwata, M.; Higashimura, H.; Anpo, M.; Matsuoka, M. Visible-light-promoted photocatalytic hydrogen production by using an amino-functionalized Ti(IV) metal−organic framework. *J. Phys. Chem. C* **2012**, *116* (39), 20848−20853.
(22) Fu, Y.; Sun, D.; Chen, Y.; Huang, R.; Ding, Z.; Fu, X.; Li, Z. An amine-functionalized titanium metal-organic framework photocatalyst with visible-light-induced activity for CO_2 reduction. *Angew. Chem., Int. Ed.* **2012**, *51* (14), 3364−3367.
(23) Zeng, L.; Guo, X.; He, C.; Duan, C. Metal−organic frameworks: versatile materials for heterogeneous photocatalysis. *ACS Catal.* **2016**, *6* (11), 7935−7947.
(24) Cavka, J. H.; Jakobsen, S.; Olsbye, U.; Guillou, N.; Lamberti, C.; Bordiga, S.; Lillerud, K. P. A new zirconium inorganic building brick forming metal organic frameworks with exceptional stability. *J. Am. Chem. Soc.* **2008**, *130* (42), 13850−13851.
(25) Bai, Y.; Dou, Y. B.; Xie, L. H.; Rutledge, W.; Li, J. R.; Zhou, H. C. Zr-based metal-organic frameworks: design, synthesis, structure, and applications. *Chem. Soc. Rev.* **2016**, *45* (8), 2327−2367.
(26) Nasalevich, M. A.; Hendon, C. H.; Santaclara, J. G.; Svane, K.; van der Linden, B.; Veber, S. L.; Fedin, M. V.; Houtepen, A. J.; van der Veen, M. A.; Kapteijn, F.; Walsh, A.; Gascon, J. Electronic origins of photocatalytic activity in d^0 metal organic frameworks. *Sci. Rep.* **2016**, *6*, 23676.
(27) Rozes, L.; Sanchez, C. Titanium oxo-clusters: precursors for a Lego-like construction of nanostructured hybrid materials. *Chem. Soc. Rev.* **2011**, *40* (2), 1006−1030.
(28) Mondloch, J. E.; Bury, W.; Fairen-Jimenez, D.; Kwon, S.; DeMarco, E. J.; Weston, M. H.; Sarjeant, A. A.; Nguyen, S. T.; Stair, P. C.; Snurr, R. Q.; Farha, O. K.; Hupp, J. T. Vapor-phase metalation by atomic layer deposition in a metal-organic framework. *J. Am. Chem. Soc.* **2013**, *135* (28), 10294−10297.
(29) Furukawa, H.; Gandara, F.; Zhang, Y. B.; Jiang, J.; Queen, W. L.; Hudson, M. R.; Yaghi, O. M. Water adsorption in porous metal-organic frameworks and related materials. *J. Am. Chem. Soc.* **2014**, *136* (11), 4369−4381.
(30) Yuan, S.; Chen, Y. P.; Qin, J. S.; Lu, W. G.; Zou, L. F.; Zhang, Q.; Wang, X.; Sun, X.; Zhou, H. C. Linker installation: engineering pore environment with precisely placed functionalities in zirconium MOFs. *J. Am. Chem. Soc.* **2016**, *138* (28), 8912−8919.
(31) Qin, J. S.; Yuan, S.; Alsalme, A.; Zhou, H. C. Flexible zirconium MOF as the crystalline sponge for coordinative alignment of dicarboxylates. *ACS Appl. Mater. Interfaces* **2017**, *9* (39), 33408−33412.
(32) Schaate, A.; Roy, P.; Godt, A.; Lippke, J.; Waltz, F.; Wiebcke, M.; Behrens, P. Modulated synthesis of Zr-based metal−organic frameworks: from nano to single crystals. *Chem. - Eur. J.* **2011**, *17* (24), 6643−6651.
(33) Meng, L.; Cheng, Q.; Kim, C.; Gao, W. Y.; Wojtas, L.; Chen, Y. S.; Zaworotko, M. J.; Zhang, X. P.; Ma, S. Crystal engineering of a microporous, catalytically active fcu topology MOF using a custom-designed metalloporphyrin linker. *Angew. Chem., Int. Ed.* **2012**, *51* (40), 10082−10085.
(34) Stoeck, U.; Krause, S.; Bon, V.; Senkovska, I.; Kaskel, S. A highly porous metal-organic framework, constructed from a cuboctahedral super-molecular building block, with exceptionally high methane uptake. *Chem. Commun.* **2012**, *48* (88), 10841−10843.
(35) Xue, D. X.; Cairns, A. J.; Belmabkhout, Y.; Wojtas, L.; Liu, Y.; Alkordi, M. H.; Eddaoudi, M. Tunable rare-earth fcu-MOFs: a platform for systematic enhancement of CO_2 adsorption energetics and uptake. *J. Am. Chem. Soc.* **2013**, *135* (20), 7660−7667.
(36) Li, M.; Li, D.; O'Keeffe, M.; Yaghi, O. M. Topological analysis of metal-organic frameworks with polytopic linkers and/or multiple building units and the minimal transitivity principle. *Chem. Rev.* **2014**, *114* (2), 1343−1370.
(37) Gomes Silva, C.; Luz, I.; Llabres i Xamena, F. X.; Corma, A.; Garcia, H. Water stable Zr-benzenedicarboxylate metal-organic frameworks as photocatalysts for hydrogen generation. *Chem. - Eur. J.* **2010**, *16* (36), 11133−11138.
(38) Sun, D.; Fu, Y.; Liu, W.; Ye, L.; Wang, D.; Yang, L.; Fu, X.; Li, Z. Studies on photocatalytic CO_2 reduction over NH_2-UiO-66(Zr) and its derivatives: towards a better understanding of photocatalysis on metal-organic frameworks. *Chem. - Eur. J.* **2013**, *19* (42), 14279−14285.
(39) Hendon, C. H.; Tiana, D.; Fontecave, M.; Sanchez, C.; D'Arras, L.; Sassoye, C.; Rozes, L.; Mellot-Draznieks, C.; Walsh, A. Engineering the optical response of the titanium-MIL-125 metal-organic framework through ligand functionalization. *J. Am. Chem. Soc.* **2013**, *135* (30), 10942−10945.

DOI: 10.1021/acscentsci.7b00497
ACS Cent. Sci. 2018, 4, 105−111